

RSC Advances



This is an *Accepted Manuscript*, which has been through the Royal Society of Chemistry peer review process and has been accepted for publication.

Accepted Manuscripts are published online shortly after acceptance, before technical editing, formatting and proof reading. Using this free service, authors can make their results available to the community, in citable form, before we publish the edited article. This *Accepted Manuscript* will be replaced by the edited, formatted and paginated article as soon as this is available.

You can find more information about *Accepted Manuscripts* in the [Information for Authors](#).

Please note that technical editing may introduce minor changes to the text and/or graphics, which may alter content. The journal's standard [Terms & Conditions](#) and the [Ethical guidelines](#) still apply. In no event shall the Royal Society of Chemistry be held responsible for any errors or omissions in this *Accepted Manuscript* or any consequences arising from the use of any information it contains.



Journal Name

ARTICLE

Experimental and theoretical studies of Triisopropanolamine as an inhibitor for aluminum alloy in 3% NaCl solution

Received 00th January 20xx,
Accepted 00th January 20xx

DOI: 10.1039/x0xx00000x

www.rsc.org/

Xiaolei Ren^a, Shenying Xu^{a,b}, Siyi Chen^a, Nanxi Chen^a, Shengtao Zhang^{a*}

The inhibition performance and mechanism of Triisopropanolamine (TIPA) for the corrosion of aluminum alloy in 3% NaCl solution were investigated using weight loss method, potentiodynamic polarization, electrochemical impedance spectroscopy (EIS) and scanning electron microscope (SEM). The electrochemical results revealed that TIPA was an effective inhibitor and the inhibition efficiency increased with the increasing concentrations of TIPA, which was further confirmed by SEM observation. Potentiodynamic polarization studies revealed that TIPA acted as the mixed-type inhibitor. The adsorption of TIPA on aluminum surface obeyed Langmuir thermodynamic–kinetic model, and the thermodynamic and kinetic parameters meant that the interaction between the inhibitor and the surface of aluminum alloy involved both physisorption and chemisorption. Moreover, the theoretical calculation was used to investigate inhibition mechanism of the studied inhibitor. The results showed that TIPA molecule could adsorb on Al substrate spontaneously and chelate with Al atom due to the hydroxyl group.

1. Introduction

Aluminum alloys exhibit excellent mechanical and physical properties as structural materials and thus they are widely applied for automotive industry, aircrafts, medical appliances, and electronic equipment. Nevertheless, they are easily corroded due to the complex microstructure and the presence of intermediate metal phase in aggressive conditions^{1–3}. Thus, the surface of aluminum alloys have to be processed to protect the alloy substrate before application.

In recent years, many scientists have studied aluminum alloys protection by inorganic salts⁴. Merten and his coworkers developed magnesium-rich primers as a coating for AA 2024-T3⁵. Zaid studied sodium metabisulfite as environmentally friendly inhibitor for aluminum alloy⁶. The salts of rare earth elements have also been found to provide the effective corrosion inhibition for aluminum alloys^{7–10}. Besides, the organic molecules were also used to protect aluminum alloys.

The use of the organic molecules as the inhibitors is one of the

convenient and economic methods to prevent corrosion of metal^{11–13}. These organic inhibitors are usually adsorbed on the metal surface via the formation of a coordinate covalent bond (chemical adsorption) or the electrostatic interaction between the metal and inhibitor (physical adsorption)¹⁴. The organic molecules would be the candidates for the effective inhibitors, if they contained heteroatoms with electronic lone pair (N, O, S and P), or p systems, or conjugated bonds, or aromatic rings^{15, 16}.

Triisopropanolamine (TIPA), a tertiary alkanol amine invented in recent years, is widely used as a grinding chemical in the clinker comminution process to reduce the agglomeration in the ball mill, and to modify the particle distribution of the finished cement¹⁷. TIPA contains N, O heteroatoms with electronic lone pair, which can interact with Al substrate. While so far, there are few reports to use it as an inhibitor for aluminum alloy.

In order to further verify the mechanism of corrosion inhibition on substrate surface, theoretical chemistry has been demonstrated to be a powerful tool¹⁸. Thus, the quantum chemical calculation and molecular dynamics simulation were used to investigate a correlation between the molecular structure and the inhibition efficiency of an organic compound¹⁹. Therefore, it is worthwhile to compute the structural parameters of the inhibitor which could affect its adsorption on metal including the highest occupied molecular orbital energy (E_{HOMO}), the lowest unoccupied molecular orbital (E_{LUMO}), etc.

^a College of Chemistry and Chemical Engineering, Chongqing University, No. 174 Shazhengjie, Shapingba, Chongqing, 400044, China Address here.

^b College of Chemistry and Chemical Engineering, Yibin University, No. 8 Jiushenglu, Yibin, Sichuan, 644000, China Address here.

* Footnotes relating to the title and/or authors should appear here. Electronic Supplementary Information (ESI) available: [details of any supplementary information available should be included here]. See DOI: 10.1039/x0xx00000x

In this study, an organic molecule triisopropanolamine (TIPA) was studied as an efficiency inhibitor for aluminum alloy in 3% NaCl solution. The adsorption type was studied by weight loss method. The corrosion efficiency was studied using potentiodynamic polarization curves and electrochemical impedance spectroscopy (EIS). The morphologies of aluminum with and without inhibitor were studied by scanning electron microscope (SEM). The effect of inhibitor concentration was investigated. The theoretical calculation parameters of the inhibitor molecules and aluminum were calculated using density functional theory (DFT).

2. Experimental methods

2.1 Materials and samples preparation

The material used in this study was commercial aluminum alloy ADC12 provided from Xinren Technology Company. The specimens were embedded in epoxy resin with dimensions of 10 mm × 10 mm × 10 mm. The total square area of the specimens exposed to the investigated solution was 1 cm². Prior to all measurements, the each specimen surface was successively abraded with 400, 800, 1200, 2000 grit silicon carbide papers at first. Then, it was degreased with acetone for 2 min, ultrasonically cleaned in ethanol for 2 min, and rinsed in distilled water at room temperature. During the weight loss and electrochemical measurements, the temperature of solution was controlled by a water thermostat, and all the experiments were open to air and carried out under static conditions.

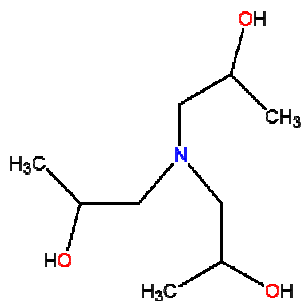


Fig. 1 Molecular structure of triisopropanolamine

The corrosive solution (3% NaCl) was prepared using analytical grade sodium chloride and distilled water. The molecular formula of investigated inhibitor triisopropanolamine (C₉H₂₁NO₃, TIPA) was shown in Fig. 1. The concentration range of inhibitor varied from 0.5–2.0 mM, and the solution in the absence of inhibitor was taken as the blank for comparison.

2.2 Weight loss measurements

Square aluminum alloy specimens with dimensions 20 mm × 20 mm × 10 mm were used for weight loss measurements. The specimens in triplicate for each inhibitor concentration were accurately weighted and then immersed in 3% NaCl solution for 24 h at 298 K. After that, the specimens were withdrawn, scrubbed with bristle

brush, cleaned by distilled water and acetone, then dried and weighed. The corrosion rate (v), inhibition efficiency (η) and surface coverage (θ) were calculated from the following equations:

$$v = \frac{\Delta W}{St} = \frac{W_1 - W_2}{St} \quad (\text{eq. 1})$$

$$\eta = \frac{v_0 - v}{v_0} \times 100\% \quad (\text{eq. 2})$$

$$\theta = \frac{v_0 - v}{v_0} \quad (\text{eq. 3})$$

where W_1 and W_2 are the weight of specimens before and after immersion, respectively, ΔW is the average weight loss (mg), S is the total surface area of the specimen (cm²), t is the immersion time (h), v_0 and v are corrosion rates in the absence and presence of inhibitors, respectively.

2.3 Electrochemical experiments

All the electrochemical experiments were performed with CHI660D electrochemical workstation in a typical three-electrode cell system. A bare aluminum electrode and a platinum electrode were used as the working electrode (WE) and the counter electrode (CE), respectively. Then a saturated calomel electrode (SCE) with a luggin capillary was worked as the reference electrode. Prior to each measurement, the working electrode was immersed in corrosive media for 2500 s until reach a steady state. All potential values were referred to SCE in this study. Potentiodynamic polarization curves were obtained by scanning the electrode potential automatically from –250 to +250 mV versus open circuit potential (OCP) at the scan rate of 2 mV s⁻¹. Electrochemical impedance spectroscopy (EIS) measurements were obtained over a frequency range from 100 kHz to 10 mHz. The amplitude of ac excitation signal was 5 mV over the OCP. The EIS data were analysed and fitted by Zsimpwin 3.10 software. The inhibitive efficiency (η) was respectively calculated from potentiodynamic polarization curves and EIS as follows:

$$\eta = \frac{I_{corr,0} - I_{corr}}{I_{corr}} \times 100\% \quad (\text{eq. 4})$$

where $I_{corr,0}$ and I_{corr} are the corrosion current densities without and with inhibitor, respectively.

$$\eta = \frac{R_{ct} - R_{ct,0}}{R_{ct}} \times 100\% \quad (\text{eq. 5})$$

where $R_{ct,0}$ and R_{ct} are the charge transfer resistances without and with inhibitor, respectively.

2.4 Surface characterization

In order to get insight into the changes on surface of corrosive samples before and after the addition of inhibitor, the aluminum specimens were first immersed in 3% NaCl in the absence and presence of 2 mM TIPA for 4 h at room temperature, respectively, then taken out from the test solution, cleaned with doubly-distilled water and dried with air. The surface morphology of the mild aluminum samples in the absence and presence of inhibitor were investigated by field emission scanning electron microscopy (FE-SEM) technique using JEOL-JSM-7800F -Japan.

2.5 Theoretical methods

Quantum chemical calculations were carried out by using Gaussian 03 software. TIPA molecule was fully optimized by density functional theory (DFT) using B3LYP functional with 6-311++G (d,p) basis set in gas phase. Quantum chemical parameters including the energy of highest occupied molecular orbital (E_{HOMO}) and the energy lowest unoccupied molecular orbital (E_{LUMO}) were calculated.

Molecular dynamics simulation of the interaction between a single inhibitor molecule and the aluminum surface was performed using Forcite module. COMPASS (condensed phase optimized molecular potentials for atomistic simulation studies) was used to optimize the structures of all the components in the studied system through in force field method. The Al crystal was cleaved along the (111) plane. Temperature was fixed at 298 K, with NVT ensemble, with a time step of 1 fs and simulation time of 500 ps. The system was quenched every 600 steps with the Al (111) surface atoms constrained. The optimized structure of the inhibitor molecule was used for the simulation.

3. Results and discussion

3.1 Weight loss

3.1.1 Effect of inhibitor concentration

Table 1 Corrosion parameters obtained from weight loss measurements of aluminum alloy after 24 h immersion in 3% NaCl solution with and without addition of various concentrations of TIPA at 298 K.

Concentration (mM)	v ($\text{mg cm}^{-2} \text{h}^{-1} \times 10^{-3}$)	θ	η (%)
0	5.5	-	-
0.5	2.0	0.64	63.6
1.0	1.8	0.67	67.5
1.5	0.7	0.87	87.3
2.0	0.4	0.92	92.3

The inhibitive effect of TIPA at different concentration on the aluminum alloy surface in 3% NaCl at 298 K was investigated by weight loss measurement. Relationship between corrosion rate (v) and concentration (C) of TIPA was shown in Fig. 2, and the corrosion rate v ($\text{mg cm}^{-2} \text{h}^{-1}$), the surface coverage θ and the values of inhibition efficiency η were listed in Table 1. It is shown that the corrosion rate (v) decreases with increasing inhibitor concentration (Fig. 2) and the inhibition efficiency η (%) increases with increasing

inhibitor concentration. At 2 mM concentration, the inhibition efficiency reaches the maximal value (92.3%). This behaviour can be attributed to the increase in adsorption of TIPA at the metal/solution interface as the concentration increases²⁰.

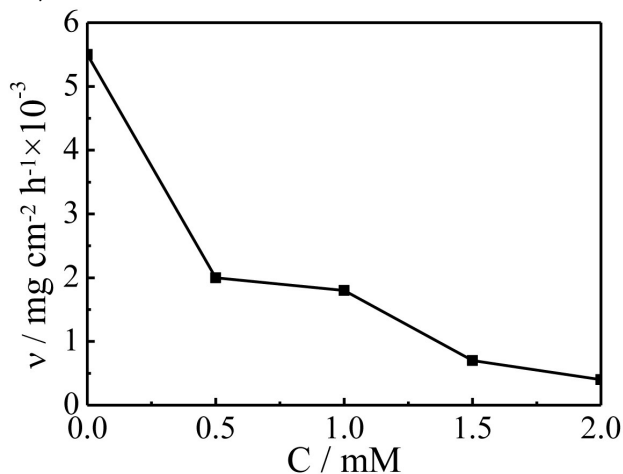


Fig. 2 Relationship between corrosion rate (v) and concentration (C) of TIPA in 3% NaCl at 298 K obtained by weight loss measurement.

3.1.2 Adsorption isotherm and thermodynamic calculations

In order to study the interaction mechanism between the inhibitor and the metal surface, the adsorption isotherm and thermodynamic calculations were studied. Two major categories of interaction can be used to describe the adsorption behaviour of the inhibitor, the one is physisorption, which occurs between the active positive centres on the metal surface. And the other one is chemisorption, it is due to the formation of coordination bonds between the inhibitor molecules and metal surface, through the electronic lone pair of N, O and S atoms^{21, 22}. In this study, some adsorption isotherms including Langmuir, Frumkin and Temkin isotherms are applied to fit the surface coverage (θ) values at different concentrations of TIPA. According to these isotherms, θ is related to the inhibitor concentration C via following equations²³:

$$\frac{C}{\theta} = \frac{1}{K_{\text{ads}}} + c \quad (\text{Langmuir isotherm}) \quad (\text{eq. 6})$$

$$\left(\frac{\theta}{1-\theta} \right) \exp(2a\theta) = K_{\text{ads}} C \quad (\text{Frumkin isotherm}) \quad (\text{eq. 7})$$

$$\exp(-2a\theta) = K_{\text{ads}} C \quad (\text{Temkin isotherm}) \quad (\text{eq. 8})$$

where C is the concentration of inhibitor; θ is surface coverage, which has been calculated by weight loss measurement and listed in Table 1; K_{ads} is the adsorption equilibrium constant and “ a ” is the molecular interaction parameter.

To fit the experimental data suitably, the correlation coefficient (R^2) was used and the best fit was obtained from the

Langmuir isotherm (Fig. 3), which suggests that the adsorption process of TIPPA on mild steel surface in 3% NaCl solution obeys the Langmuir adsorption isotherm. This model proposes that the solid surface contains a fixed number of adsorption sites and each site holds one adsorbed species²⁴. Thus, the adsorption equilibrium constant (K_{ads}) is related to the standard free energy of adsorption (ΔG_{ads}^0) of the inhibitor molecule by the following equation²⁵:

$$K_{\text{ads}} = \frac{1}{55.5} \exp\left(\frac{-\Delta G_{\text{ads}}^0}{RT}\right) \quad (\text{eq. 9})$$

where R is the universal gas constant, T the thermodynamic temperature in K, and 55.5 represents the molar concentration of water in the solution. The values of K_{ads} and ΔG_{ads}^0 are 440 L/mol and -29.10 kJ/mol, respectively. The value of ΔG_{ads}^0 is -29.10 kJ/mol, which probably means that the interaction between the inhibitor and the surface of aluminum alloy involves both physisorption and chemisorption^{19, 26}.

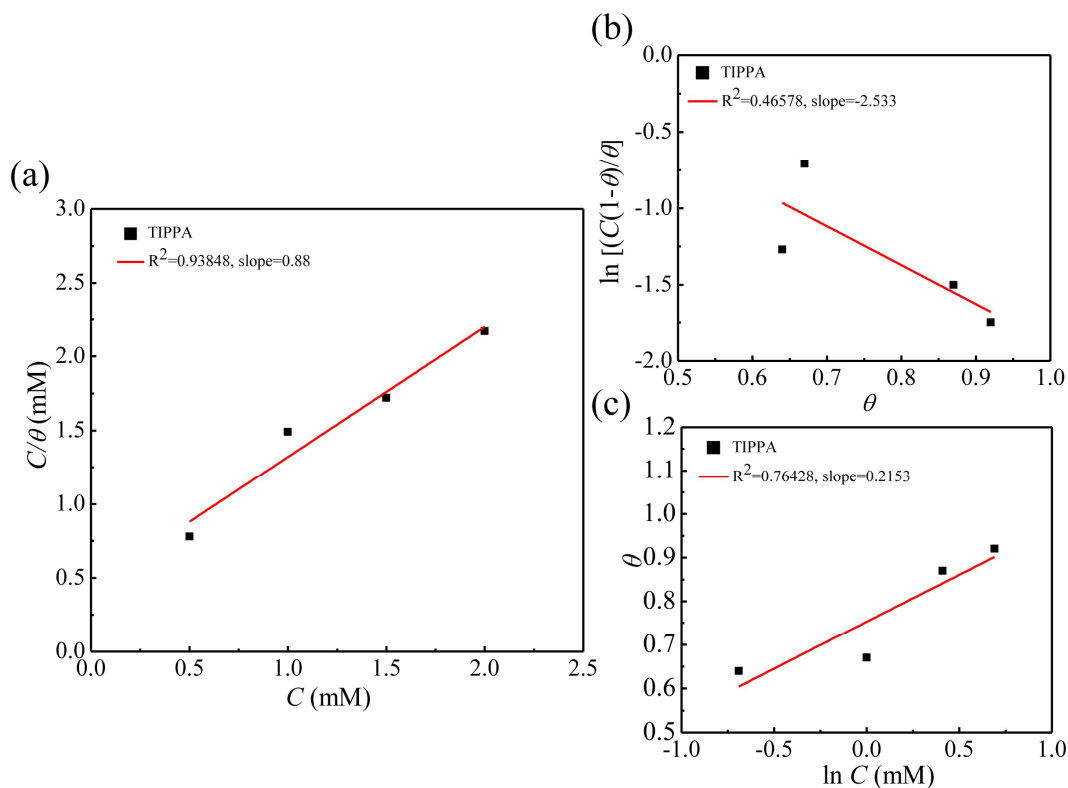


Fig. 3 Three different isotherm plots for aluminum alloy in 3% NaCl solution containing different concentrations of TIPPA at 298 K. (a) Langmuir isotherm plot, (b) Frumkin isotherm plot, (c) Temkin isotherm plot, respectively.

3.2 Potentiodynamic polarization curves

Figure 4 shows the potentiodynamic polarization curves for aluminum alloy in 3% NaCl solution in the absence and presence of TIPPA in different concentrations at 298 K. It is obvious that the polarization curves are shifted to the lower current density with the increase of the inhibitor concentration. Furthermore, the cathodic curves give rise to the parallel lines with increasing inhibitor concentration. The results show that the addition of inhibitor does not modify the oxygen evolution mechanism²⁷. The reduction of oxygen at the aluminum alloy surface takes place mainly through a charge transfer mechanism. As compared with the blank experiment, the anodic curves of the working electrode with TIPPA

shift obviously to the direction of the current reduction, which implies that the organic compounds could also suppress the anodic reaction. Furthermore, the corrosion potential (E_{corr}) only shifts slightly, so TIPPA can be seen as the modest mixed-type inhibitor²⁸.

In order to obtain information about the kinetics of the corrosion, the representative electrochemical parameters, such as corrosion potential E_{corr} (mV/SCE), cathodic and anodic Tafel slopes β_c and β_a (mV/dec), corrosion current density I_{corr} ($\mu\text{A}/\text{cm}^2$), and inhibition efficiency η (%) values are calculated from the corresponding polarization curves. These data are shown in Table 2. It is clear that I_{corr} value decreases with increasing inhibitor concentration TIPPA. Accordingly, η increases with the increasing inhibitor concentration.

The results suggest that TIPA acts as an efficient inhibitor for aluminum alloy in 3% NaCl solution. And, this effect is due to the increase in the covered fraction of the electrode surface by the adsorption through nonbonding electron pairs from oxygen atoms. It is expected that a higher coverage of the inhibitor film on the aluminum alloy surface is obtained at a higher inhibitor concentration.

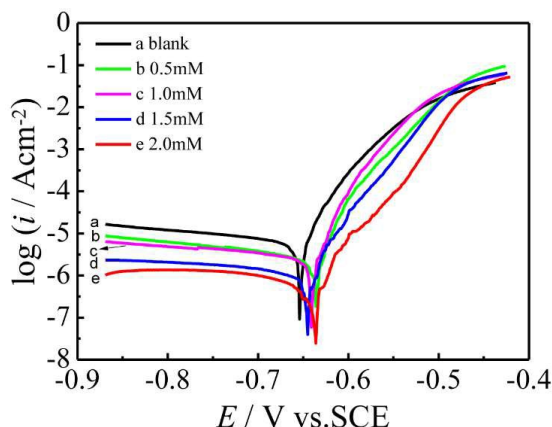


Fig. 4 Potentiodynamic polarization curves for aluminum alloy in 3% NaCl solution with and without different concentration of TIPA at 298 K.

Table 2 The electrochemical parameters for aluminum alloy in 3% NaCl solution without and with different concentration of TIPA at 298 K.

C (mM)	E_{corr} (V)	β_c (mV/sec)	β_a (mV/sec)	I_{corr} ($\mu\text{A}/\text{cm}^2$)	η (%)
0	-0.654	492.4	33.53	7.94	-
0.5	-0.636	479.8	29.53	3.27	58.8
1.0	-0.641	514.4	26.52	3.04	61.7
1.5	-0.645	564.7	33.94	1.27	84.0
2.0	-0.636	463.4	38.85	0.81	89.8

3.2 Electrochemical impedance spectroscopy

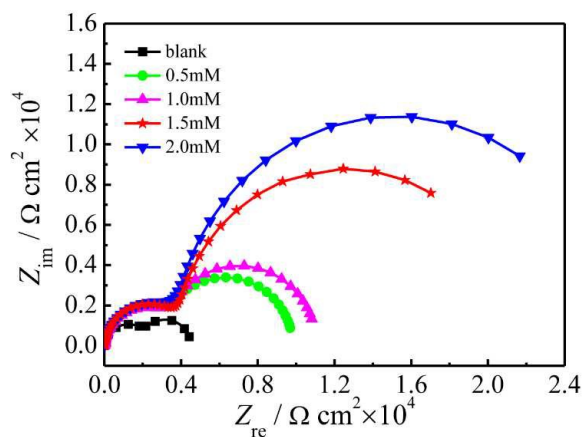


Fig. 5 Nyquist impedance diagrams for aluminum alloy obtained at 298 K in 3% NaCl solution containing different concentrations of TIPA.

In order to acquire more information about corrosion mechanism, Nyquist plots for aluminum alloy after immersed in 3% NaCl solution in the absence and presence of different concentrations of TIPA at 298 K are given in Fig. 5. It is clear that all the impedance spectra exhibit two capacitive loops, which suggests that the corrosion of aluminum in 3% NaCl with and without the inhibitor is not only controlled by charge transfer process, but also controlled by adsorption-desorption process of inhibitive molecules²⁹. In addition, these diagrams show a similar trend for all the tested concentrations, indicating that there is no change in the corrosion mechanism. Furthermore, the diameter of the semicircles in the presence of TIPA is larger than the one in blank solution (3% NaCl), and it increases with increasing inhibitor concentration, which could be related to the increase of surface coverage of TIPA molecule on aluminum alloy surface.

The corresponding Bode and phase angle plots recorded for aluminum electrode immersed in 3% NaCl with and without different concentrations of TIPA are given in Fig. 6. As seen from Fig. 6, Bode and phase plots indicate there is the presence of two time constants over the measured frequency as well as the existence of an equivalent circuit containing two constant phase elements in the interface of metal/solution. The increase of impedance at low frequency in Bode plot confirms the higher protection with increasing inhibitor concentration. Additionally, phase angle increased with the increase of concentrations due to more TIPA molecules adsorbed on aluminum surface at the higher concentration (Fig. 6b).

To determine the impedance parameters, electrical equivalent circuit shown in Fig. 7 is employed to simulate the obtained EIS data using ZSimpWin software. In the circuits, R_s is the solution resistance, R_{ct} is the charge transfer resistance, R_f is the film resistance, CPE is the membrane capacitance and can be described as follows²⁶:

$$Z_{CPE} = \frac{I}{Y_0 (j\omega)^n} \quad (\text{eq. 10})$$

where Y_0 is the CPE constant, n is the phase shift which can be explained as a degree of surface inhomogeneity, j is the imaginary unit and ω is the angular frequency.

According to the expression of the layer capacitance presented in the Helmholtz model³⁰:

$$C_{dl} = \frac{\epsilon^0 \epsilon S}{d} \quad (\text{eq. 11})$$

where d is the thickness of the film, S is the surface of the electrode, ϵ^0 is the permittivity of the air and ϵ is the local dielectric constant. The impedance parameters namely, R_s , R_{ct} , R_f , Y_0 , n , C_{dl} and η , are given in Table 3.

As can be seen in Table 3 that the R_{ct} value increases with increasing inhibitor concentration while the C_{dl} value exhibits

reverse dependence, meanwhile the R_f value also increases with increasing TIPA concentration, which is due to the increase of coverage on the aluminum alloy surface by the adsorption of inhibitor, leading to the better inhibition efficiencies. The decreased value of C_{dl} indicates the reducing in local dielectric constant and/or an increase in the thickness of the electrical double layer, suggesting that the inhibitor molecules act by adsorption on the

metal/solution interface³¹. The values of n are close to one, which shows that the interface behaves nearly capacitive. The inhibition efficiency at 2 mM reaches the maximal value of 91.5%. The electrochemical experiments reveal that the inhibition efficiencies obtained from EIS and polarization curves are in reasonably good agreement.

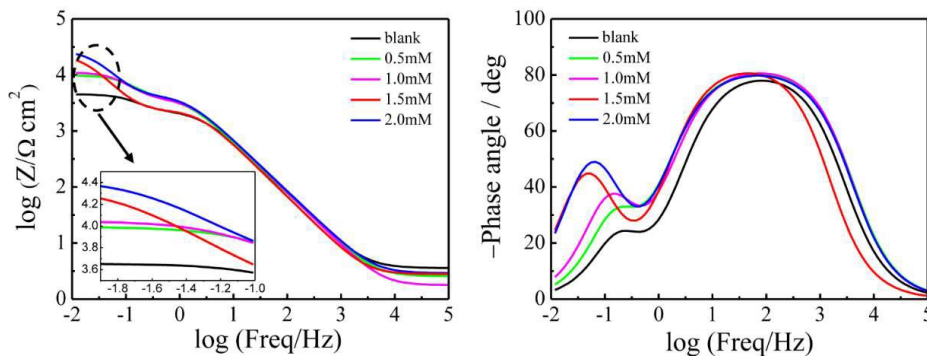


Fig. 6 Bode (a) and phase angle plots (b) of aluminum alloy in 3% NaCl solution in the absence and presence of different concentrations of TIPA at 298 K.

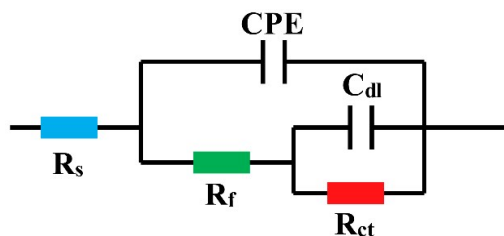


Fig. 7 Equivalent circuit used to fit the EIS loop.

Table 3 EIS parameters for aluminum alloy in 3% NaCl solution with and without different concentrations of inhibitor at 298 K.

Concentration (mM)	R_s ($\Omega \text{ cm}^2$)	CPE		R_f ($\Omega \text{ cm}^2$)	C_{dl} ($\mu\text{F cm}^{-2}$)	R_{ct} ($\text{k}\Omega \text{ cm}^2$)	η (%)
		Y_0 ($\text{S} \cdot \text{cm}^{-2} \cdot \text{s}^{-n} \times 10^{-5}$)	n				
0	3.58	3.56	0.91	2410	5.91	2.09	-
0.50	2.54	3.41	0.92	4081	3.37	4.25	50.8
1.00	1.77	3.06	0.94	4155	3.23	8.26	74.6
1.50	2.78	3.34	0.94	4497	3.19	20.94	90.0
2.00	3.89	2.96	0.92	4778	2.79	24.75	91.5

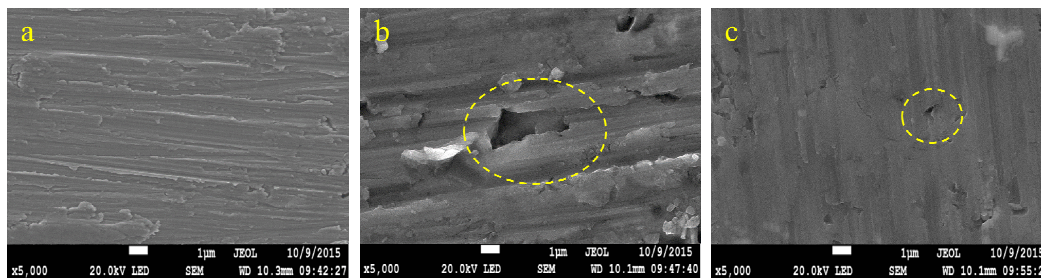


Fig. 8 SEM micrographs of aluminum surface. (a) abraded without immersion in test solution; (b) after 4 h immersion in 3% NaCl without inhibition; (c) after 4 h immersion in 3% NaCl containing 2 mM of the inhibitor TIPA.

3.4 SEM analyses

The surface morphology of the sample before immersion in 3% NaCl solution showed a freshly abraded aluminum surface (Fig. 8a). SEM photographs obtained from aluminum surface after the specimens immersion in 3% NaCl for 4 h in the absence and presence of 2 mM of TIPA were shown in Fig. 8b and 8c, respectively. It could be observed from Fig. 8b that the specimen surface was strongly corroded in the absence of the inhibitor. However, Fig. 8c shows that in presence of the TIPA, the rate of corrosion was suppressed, it revealed that there was a good protective film adsorbed on specimens surface, which was responsible for the inhibition of corrosion.

3.5 Theoretical calculation

3.5.1 Quantum chemical calculations

Quantum chemical calculations have a potential application towards the design and development of organic corrosion inhibitors in corrosion field^{32, 33}. Recently, density functional theory³⁴ (DFT) has been carried out in order to investigate the adsorption and inhibition mechanism that relates the molecular structure of the inhibitor and its inhibiting effect. The frontier molecule orbital density distributions of trisopropanolamine and the full optimized minimum energy geometrical configurations and are shown in Fig. 9 and Fig. 10.

According to the frontier molecular orbital theory, the formation of a transition state is due to an interaction between HOMO and LUMO of reactants. Fig. 9 shows that the electron density distribution of HOMO is located at nitrogen atom, while that of LUMO is mainly distributed in hydroxyl group.

Additionally, it can be seen that the contour and the total electron density surface mapped with electrostatic surface potential (ESP) of trisopropanolamine is shown in Fig. 10a and 10b, respectively. The negative (red) regions of the ESP are related to nucleophilic reactivity and the positive (blue) regions to electrophilic reactivity. As shown in this figure, it is clear that more electron rich regions are mainly localized around the heteroatoms¹⁹. It means that TIPA can promote the formation of a physical electrostatic interaction on the aluminum alloy surface by the hydroxyl to Al atom, and forming a coordinate covalent bond through the chemical adsorption. In this way, the aluminum surface acting as an electrophile is susceptible to attract the negatively charged sites of inhibitor molecule, and the nucleophilic centres of inhibitor molecules are normally heteroatoms with free electron

pairs, which are readily available to form chemical bonds. The possible orientation of inhibitor on the aluminum surface is shown in Fig. 11

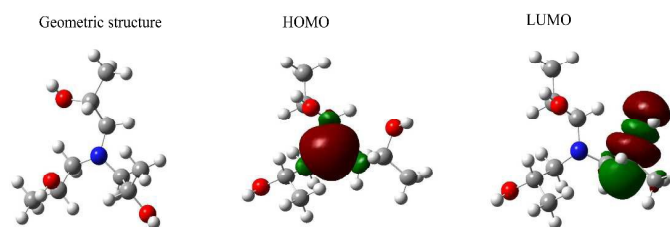


Fig. 9 Optimized geometric structure and the distributions of HOMO and LUMO for TIPA.

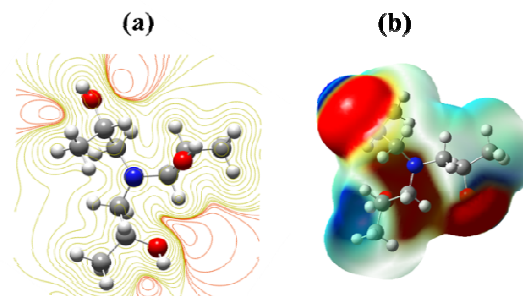


Fig. 10 Quantum chemical results of TIPA molecular calculated by the DFT method with 6-311G++(d,p) basis set: (a) contour map of electrostatic surface potential and (b) total electron density surface mapped with electrostatic potential.

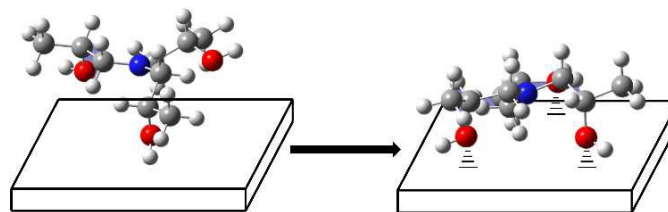


Fig. 11 Possible orientation of inhibitor on the aluminum surface.

3.5.2 Molecular dynamics simulation

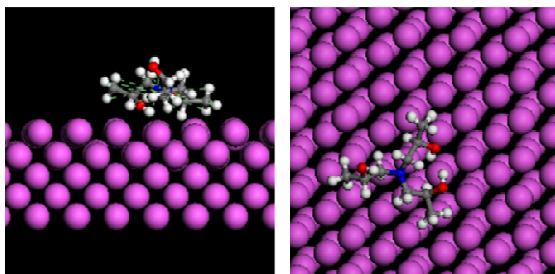


Fig. 12 The side view and the top view of the optimized equilibrium configuration of TIPA on aluminum (111) surface.

Table 4 Energy parameters for the Al surface and TIPA

E_{Al} (kJ/mol)	E_{TIPA} (kJ/mol)	$E_{Al-TIPA}$ (kJ/mol)	E_{ad} (kJ/mol)
-1.39E4	51.49	-1.40E4	-151.49

In order to further discuss the interaction between the inhibitor molecular and aluminum substrate, molecular dynamics simulation was carried out to propose the model of the adsorption structure of TIPA. Figure 12 shows the side view and the top view of the optimized equilibrium configuration of TIPA on aluminum (111) surface and the energy of TIPA and Al surface is listed in Table 4. We can see in Figure 12 that TIPA molecule tends to be absorbed in parallel on the surface through hydroxyl group, which is similar to the result of quantum chemistry calculations above. This parallel orientation can maximize the contacting areas between the inhibitor molecule and aluminum surface to enhance the anticorrosion performance³⁵. Furthermore, the value of E_{ad} is negative which explains TIPA molecule can spontaneously adsorb on Al surface³⁶. Thus, we can indicate that the spontaneous adsorption effects occur through physical electrostatic interaction and coordinate bonds, which is formed by the heteroatoms.

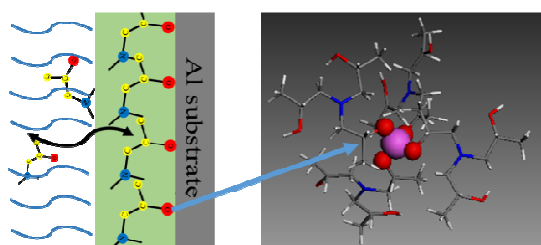
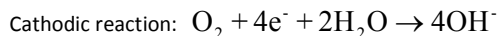


Fig. 13 The adsorption structure of TIPA on aluminum alloy surface.

3.6 Mechanism of corrosion inhibition

The corrosion progress would take place once the bare aluminum was putted in 3% NaCl solution. The reactions were shown as follow:



However, as TIPA is added into the aggressive solution, the progress of corrosion is prevented. TIPA molecule spontaneously adsorbs at metal/solution interface, due to that hydroxyl groups can produce physical electrostatic interaction and chemical chelate with aluminum by the strong electron-donating effect, as shown in Fig. 13. Thus, it decreases the extent of the dissolution reaction by occupying the active sites. So the aluminum surface covered with many TIPA molecules. Furthermore, the fraction of coverage increases with the increasing TIPA concentration.

Conclusions

The electrochemical results show that TIPA as a modest mixed-type inhibitor can not only inhibit the cathodic process but also the anodic process on the corrosion of aluminum alloy in 3% NaCl solution, and its inhibitive efficiency increases with its incremental concentrations. The adsorption of TIPA molecules on the aluminum alloy surface obeys Langmuir adsorption isotherm. The results obtained from gravimetric and electrochemical techniques are in nice agreement with each other. Furthermore, the theoretical calculations reveal that TIPA exhibits a better inhibitive performance due to the strong electron-donating effect of hydroxyl group, and it mainly adsorbs on the substrate surface through O atom. The molecular dynamics simulation explains the adsorption occurred spontaneously.

Acknowledgements

This work was supported by Natural Science Foundation of China (No. 21376282)

References

- 1 Y. Totik, R. Sadeler, I. Kaymaz, M. Gavagli. *J Mater Process Tech*, 2004, **147**, 60.
- 2 B. E. Rivera, B. Y. Johnson, M. J. O'Keefe, W. G. Fahrenholtz. *Surf Coat Tech*, 2004, **176**, 349.
- 3 C. Y. Bai, Y. H. Chou, C. L. Chao, S. J. Lee, M. D. Ger. *Journal of Power Sources*, 2008, **183**, 174.
- 4 E. E. Abd El Aal, S. Abd El Wanees, A. Farouk, S. M. Abd El Haleem. *Corros Sci*, 2013, **68**, 14.
- 5 B. J. E. Merten, D. Battocchi, G. P. Bierwagen. *Prog Org Coat*, 2015, **78**, 446.
- 6 B. Zaid, N. Maddache, D. Saidi, N. Souami, N. Bacha, A. S. Ahmed. *J Alloy Compd*, 2015, **629**, 188.
- 7 M. A. Arenas, M. Bethencourt, F. J. Botana, J. de Damborenea, M. Marcos. *Corros Sci*, 2001, **43**, 157.
- 8 A. Aballe, M. Bethencourt, F. J. Botana, M. Marcos, R. M. Osuna. *Electrochim Acta*, 2002, **47**, 1415.
- 9 E. A. Matter, S. Kozhukharov, M. Machkova, V. Kozhukharov. *Corros Sci*, 2012, **62**, 22.
- 10 T. H. Hu, H. W. Shi, T. Wei, F. C. Liu, S. H. Fan, E. H. Han. *Corros Sci*, 2015, **95**, 152.
- 11 K. R. Ansari, M. A. Quraishi, A. Singh. *J Ind Eng Chem*, 2015, **25**,

- 89.
- 12 Y. J. Qiang, S. T. Zhang, S. Y. Xu, L. L. Yin. *Rsc Adv*, 2015, **5**, 63866.
- 13 M. A. Hegazy, S. S. A. El Rehim, A. M. Badawi, M. Y. Ahmed. *Rsc Adv*, 2015, **5**, 49070.
- 14 C. M. Goulart, A. Esteves-Souza, C. A. Martinez-Huitle, C. J. F. Rodrigues, M. A. M. Maciel, A. Echevarria. *Corros Sci*, 2013, **67**, 281.
- 15 S. M. Abd El Haleem, S. Abd El Wanees, E. E. Abd El Aal, A. Farouk. *Corros Sci*, 2013, **68**, 1.
- 16 A. Doner, E. A. Sahin, G. Kardas, O. Serindag. *Corros Sci*, 2013, **66**, 278.
- 17 H. Huang, X. D. Shen. *Constr Build Mater*, 2014, **65**, 360.
- 18 G. Gece. *Corros Sci*, 2008, **50**, 2981.
- 19 D. Daoud, T. Douadi, H. Hamani, S. Chafaa, M. Al-Noaimi. *Corros Sci*, 2015, **94**, 21.
- 20 I. B. Obot, N. O. Obi-Egbedi. *Curr Appl Phys*, 2011, **11**, 382.
- 21 S. D. Deng, X. H. Li, H. Fu. *Corros Sci*, 2011, **53**, 822.
- 22 I. Ahamad, R. Prasad, M. A. Quraishi. *Corros Sci*, 2010, **52**, 3033.
- 23 M. Lebrini, M. Lagrenee, H. Vezin, L. Gengembre, F. Bentiss. *Corros Sci*, 2005, **47**, 485.
- 24 A. M. Badiea, K. N. Mohana. *Corros Sci*, 2009, **51**, 2231.
- 25 X. W. Zheng, S. T. Zhang, W. P. Li, L. L. Yin, J. H. He, J. F. Wu. *Corros Sci*, 2014, **80**, 383.
- 26 M. A. Hegazy, M. Abdallah, M. K. Awad, M. Rezk. *Corros Sci*, 2014, **81**, 54.
- 27 X. W. Zheng, S. T. Zhang, W. P. Li, M. Gong, L. L. Yin. *Corros Sci*, 2015, **95**, 168.
- 28 S. A. Umoren, Y. Li, F. H. Wang. *Corros Sci*, 2010, **52**, 2422.
- 29 S. A. Umoren, Y. Li, F. H. Wang. *Corros Sci*, 2010, **52**, 1777.
- 30 D. Wang, B. Xiang, Y. P. Liang, S. Song, C. Liu. *Corros Sci*, 2014, **85**, 77.
- 31 Z. H. Tao, S. T. Zhang, W. H. Li, B. R. Hou. *Corros Sci*, 2009, **51**, 2588.
- 32 L. Guo, S. T. Zhang, W. P. Li, G. Hu, X. Li. *Mater Corros*, 2014, **65**, 935.
- 33 A. L. R. Silva, A. Cimas, M. D. M. C. R. da Silva. *J Chem Thermodyn*, 2013, **57**, 212.
- 34 P. J. Stephens, F. J. Devlin, C. F. Chabalowski, M. J. Frisch. *J Phys Chem-U*, 1994, **98**, 11623.
- 35 H. Heinz, B. L. Farmer, R. B. Pandey, J. M. Slocik, S. S. Patnaik, R. Pachter, et al. *J Am Chem Soc*, 2009, **131**, 9704.
- 36 E. E. Oguzie, K. L. Oguzie, C. O. Akalezi, I. O. Udeze, J. N. Ogbulie, V. O. Njoku. *Acs Sustain Chem Eng*, 2013, **1**, 214.